

# Critical and many-body localized phases under disorders with power-law correlations

Takahiro Orito<sup>1,\*</sup>, Yoshihito Kuno<sup>2,\*</sup> and Ikuo Ichinose<sup>1</sup>

<sup>1</sup>*Department of Applied Physics, Nagoya Institute of Technology, Nagoya, 466-8555, Japan and*

<sup>2</sup>*Department of Physics, Graduate School of Science, Kyoto University, Kyoto, 606-8502, Japan*

(Dated: March 2, 2020)

We study effects of correlated disorders in a typical many-body-localized (MBL) system, i.e., an anti-ferromagnetic spin chain in a random external magnetic field. Controlling the correlation of disorders is feasible in recent real experimental systems such as cold atoms in an optical lattice. Effects of correlations in disorders in MBL systems, however, have not been clarified theoretically so far. In this work, we consider power-law-correlated disorders for the random external magnetic field such as  $\langle \eta_j \eta_{j+\ell} \rangle \propto (1 + \ell^2)^{-\gamma/2}$ , where  $\{\eta_j\}$  are random variables and  $\gamma$  is an exponent. We numerically investigate the localization properties of the system rather in detail. The power-law-type disorders induce localization properties essentially different from those of a uniform white-noise disorder, the MBL properties of which have been extensively studied. Notably, we find that the power-law-type disorders strongly enhance a critical phase, i.e., the critical regime seems to survive as a robust phase even in the thermodynamic limit. The phase boundary between MBL and critical phases is strongly influenced by the exponent and strength of disorder correlations, i.e., disorders with longer correlations (smaller  $\gamma$ ) enhance the critical phase more strongly. In addition, we also systematically investigate entanglement properties under long-range-correlated disorders and find that the properties of disorders influence the time evolution of entanglement entropy significantly.

PACS numbers:

## I. INTRODUCTION

Many-body localization (MBL) attracts a lot of attentions and interests in condensed matter and quantum information physics these days [1–3]. Recent theoretical studies have developed novel points of view such as entanglement dynamics, thermalization properties, and the relationship to quantum integrable systems. Development of numerical simulation techniques plays an important role for such trends. In the experimental side, various isolated quantum systems with inter-particle interactions have been constructed in experiments on ultra-cold atoms, and they ‘quantum simulate’ MBL phenomena by controlling strength of quasi-periodic disorders [4–7]. Controllable disorders and interactions between particles have the potential ability to generate various novel localization phenomena, which have not been observed in solid state materials.

In this work, we study effects of correlated disorders in a typical MBL system, i.e., anti-ferromagnetic  $S = \frac{1}{2}$  spin chain in a random external magnetic field. In particular, effects of disorders with power-law correlations are focused, which are feasible in recent experiments. [For explicit expressions of the random variables, see Eqs. (3) and (9).] In the recent studies on MBL, systems with long-range, long-range random, and power-law long-range interactions have been extensively studied by numerical methods [8–10], but research on correlated disorders has been still lacking in the study of MBL. For Anderson localization study, such power-law disorders *in non-interacting systems* have been extensively studied so

far, in particular, from the view point of the localization length and phase diagram [11–16]. However, the extensive study from the modern view point such as entanglement properties, localization dynamics and thermalization properties is still lacking. Therefore in this work, we shall investigate the effects of the power-law disorders in a systematic way from the above mentioned point of view.

We clarify that the MBL systems under power-law disorders exhibit various localization nature that is different from the system with the conventional short-range on-site random disorders. In particular, the global phase diagram, which depends on the exponent and strength of the power-law disorder, is clarified by employing the multi-fractal analysis [17, 18] and some system size scaling analysis. Notably, the global phase diagram clearly exhibits large critical regimes. This critical phase is not a numerical artifact due to the finite size effect as the conventional MBL system [19], but it seems to survive even in the thermodynamics limit. Furthermore, we investigate the dynamics of entanglement entropy for this power-law disordered system. Long-range correlated disorders change the time evolution of entanglement significantly.

This paper is organized as follows. In Sec. II, we introduce the target MBL model, the anti-ferromagnetic  $S = \frac{1}{2}$  spin chain in the random magnetic field with the long-range correlations. In Sec. III, we explain the methods to generate the power-law correlated random variables by making use of the Fourier filtering method (FFM). We carefully examine random variables generated by the FFM to find that they display the desired correlation. In Sec. IV, non-interacting systems are studied by measuring various quantities. The problem of how nature of Anderson localization changes due to the cor-

---

\*These two authors contributed equally.

related random magnetic field is carefully investigated. Section V is devoted for study on the interacting case. Various quantities are calculated numerically and obtain the phase diagram, in which a novel critical phase exists in a finite parameter region. Then, finite-size-scaling analysis is used to discuss the thermodynamic limit. In Sec. VI, the dynamics of the entanglement entropy and other related physical quantities are investigated. The obtained results support the observations in Sec. V, in particular, the existence of the critical phase. Section VII is devoted to conclusion.

## II. MODEL

In this work, we consider one of the typical canonical models for the MBL study,  $S = \frac{1}{2}$  XXZ spin model, Hamiltonian of which is given by,

$$H_S = \sum_j \frac{J_{xy}}{2} (S_j^+ S_{j+1}^- + S_j^- S_{j+1}^+) + J_z S_j^z S_{j+1}^z, \quad (1)$$

where,  $S_j^{+(-)}$  is a raising (lowering) spin operator,  $S_j^z$  is z-component spin operator, and  $J_{xy}$  and  $J_z$  are exchange coupling and z-component Ising coupling, respectively. Since the  $J_z$ -term acts as an interaction in the Jordan-Wigner fermion picture of the system [Eq. (1)], the model is expected to exhibit MBL in the presence of disorders, e.g., a random external magnetic field.

In this paper, we consider the following random magnetic field as a disorder,

$$H_d = \sum_j \eta_j S_j^z, \quad (2)$$

where  $\{\eta_j\}$  are random variables and have the following specific power-law correlation,

$$\langle \eta_j \eta_{j+\ell} \rangle_{\text{ans}} \propto (1 + \ell^2)^{-\gamma/2}. \quad (3)$$

In Eq. (3),  $\langle \dots \rangle_{\text{ans}}$  means ensemble average of the disorder  $\{\eta_i\}$ , and  $\gamma$  is a power-law exponent, which takes various values in the following study. The method of generating the correlated disorder  $\{\eta_j\}$  will be explained in Sec. III. The correlation in Eq. (3) reduces to the genuine power-law correlation  $\sim \ell^{-\gamma}$  for  $\ell \gg 1$ . The merit of the form of Eq. (3) is that the singularity for  $\ell \rightarrow 0$  in the genuine power-law correlation is safely avoided. Although the disorders of Eq. (3) slightly deviate from the genuine power-law correlation  $\ell^{-\gamma}$ , but it is a good approximation for studying localization. Some previous works studied effects of this type of disorder for Anderson localization [12, 13, 15, 16]. The localization properties of the systems depend on the parameter  $\gamma$ , and interesting phenomena have been reported for Anderson localization, e.g., the violation of Harris criterion [14], the presence of a localization-delocalization phase transition, etc. In this paper, we shall investigate how this type of disorder affect the phase diagram of the spin model of

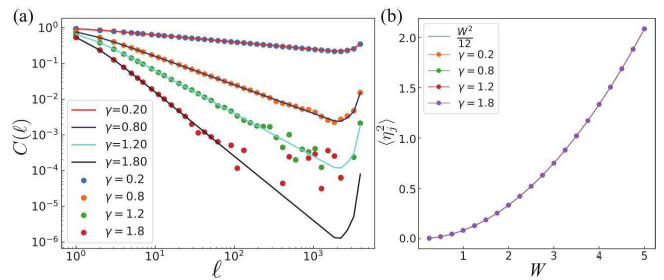


FIG. 1: (a) Numerically generated random variables with power-law correlations. (b) Variance of the generated power-law random variable as a function of  $W$ .

Eq. (1). That is, we focus on how the spatial correlation of Eq. (3) affects localization properties of the system and compare the obtained results with those of the spin model in the uniformly random external magnetic field, under which the conventional MBL occurs. To this end, we consider  $0.2 \leq \gamma \leq 2$  throughout this paper. For the practical numerical study, the XXZ model of Eq. (1) is mapped into the fermion system through the Jordan-Wigner transformation. Throughout this paper, we set  $J_{xy} = 1$  and consider the half-filled case in the fermion picture, i.e., the  $\sum_j S_j^z = 0$  sector in the XXZ model.

## III. RANDOM VARIABLES WITH POWER-LAW CORRELATIONS

In this section, we explain the methods generating random variables  $\{\eta_i\}$ . In general, the power-law random variables can be produced by employing the FFM, as first discussed in Ref. [20]. Later, modification of the FFM was developed in Ref. [12], and variance-parameterized versions of the power-law disorder were discussed in Ref. [13]. In this paper, we employ the power-law disorders with the controllable variance parameterized by  $W$ . The value of  $W$  is proportional to the strength of the disorder. We shall investigate the  $W$ -dependence of various physical quantities by the numerical study in later sections. Therefore, we employ the FFM with a rescale-variance technique, which was proposed in Ref. [13].

To numerically generate  $\{\eta_j\}$  for the system with size  $L$ , we start with an ensemble of white-noise random variables  $\{u_j\}$  ( $j = 1, \dots, L$ ), whose correlation is simply given by,

$$\langle u_j u_{j+\ell} \rangle_{\text{ans}} = \delta_{j,j+\ell}. \quad (4)$$

From the ensemble  $\{u_j\}$ , we can construct random variables  $\{\bar{\eta}_j\}$ , which have the following power-law correlation,

$$C(\ell) = \langle \bar{\eta}_j \bar{\eta}_{j+\ell} \rangle_{\text{ans}} = (1 + \ell^2)^{-\gamma/2}. \quad (5)$$

To generate  $\{\bar{\eta}_j\}$ , we use the Fourier form of the above

correlation, i.e.,

$$C(\ell) \xrightarrow{\text{IFT}} S(k) = \langle \bar{\eta}(k) \bar{\eta}(-k) \rangle_{\text{ans}}, \quad (6)$$

where IFT denotes the integer Fourier transformation (IFT). Then the Fourier counterpart of  $\{\bar{\eta}_j\}$  can be obtained from the Fourier counterpart of  $\{u_j\}$  [20],

$$\bar{\eta}(k) = S^{1/2}(k)u(k). \quad (7)$$

Then by applying the IFT to  $\{\bar{\eta}(k)\}$ , we obtain  $\{\bar{\eta}_j\}$  with the power-law correlation of Eq. (5). Furthermore according to Ref. [13], we can add disorder strength to  $\{\bar{\eta}_j\}$  by imposing a normalization condition on the variance of the random variables  $\{\bar{\eta}_j\}$ . It is achieved by rescaling  $\{\bar{\eta}_j\}$  as

$$\eta_j = \frac{W}{\sqrt{12\sigma_L}}(\bar{\eta}_j - \langle \bar{\eta} \rangle_L), \quad (8)$$

where  $\sigma_L$ ,  $\langle \bar{\eta} \rangle_L$  are the variance and the mean value of  $\bar{\eta}_j$ 's  $\{\{\bar{\eta}_1, \dots, \bar{\eta}_L\}\}$ , respectively. We obtain a sequence of disorders  $\{\eta_j\}$  for the target system size. Its variance is controlled by  $W$  as

$$\langle \eta_j^2 \rangle_{\text{ans}} = W^2/12, \quad \text{with } \langle \eta_j \rangle_{\text{ans}} = 0. \quad (9)$$

For Anderson localization in weak-disorder cases, it is known that localization length of energy eigen states depends on the variance of disorder [21]. We expect that this observation is also applicable to MBL. In this sense, the variance  $W$  is one of key parameters that control localization of the system with the power-law correlated disorder. In the later numerical studies, we regard  $W$  as the disorder-strength parameter.

We numerically generate variables  $\{\eta_j\}$  for various values of  $\gamma$ . In Fig. 1(a), we show the behavior of the correlation function obtained from the generated  $\{\eta_j\}$ . Fig. 1(a) shows that  $\{\eta_j\}$ 's with the power-law correlation of Eq. (5) are obtained satisfactorily. It is noted that for  $\ell \gg 1$ , the correlation of the numerically obtained  $\{\eta_j\}$  slightly deviates from the strict line of Eq. (5), but the deviation is less than  $\mathcal{O}(10^{-4})$ , therefore it is negligibly small. Figure 1(b) shows the variance of  $\{\eta_j\}$ 's as a function of  $W$ . We observe the good agreement between the numerical results and analytic expression in Eq. (9).

#### IV. XY MODEL: $J_z = 0$ CASE

We first study effects of the disorder  $\{\eta_j\}$  for the non-interacting case  $J_z = 0$  in Eq (1). To investigate the localization properties of single-particle states in the system  $H_S|_{J_z=0} + H_d$ , we calculate inverse participation ratio (IPR). The IPR for each eigenstate is defined as

$$(\text{IPR})_n = \sum_j |\langle j | \psi_n \rangle|^4, \quad (10)$$

where  $|j\rangle$  is the localized single-particle state at site  $j$ , and  $|\psi_n\rangle$  is  $n$ -th single particle eigenstate. For localized

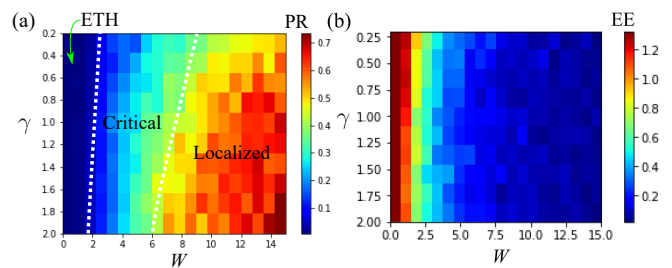


FIG. 2: (a) Averaged IPR calculated for the non-interacting case  $J_z = 0$ . The values of IPR is obtained by using single-particle states in the vicinity of the band center. (b) Averaged EE calculated for the non-interacting case  $J_z = 0$ . The EE is obtained from the groundstate wave function by the slater determinant of the half-filling system.

states, IPR is close to unity, whereas  $\text{IPR} \ll 1$  for extended states.

Here, we focus on the IPR at the band center (i.e., in the vicinity of the  $L/2$ -th state). Figure 2(a) exhibits the result of the IPR in the  $(\gamma - W)$  plane. The system size is  $L = 124$ , and the number of disorder realizations is  $N_d = 50$ . The calculations clearly show  $\gamma$ -dependence of the IPR, i.e., the power-law correlation of the disorders significantly affects the localization character. Interestingly enough, we can recognize three phases, i.e., ETH, critical and localized phases and they are connected through crossovers. In other words, it is hard to detect genuine phase transition lines separating these phases. Here, the ETH phase corresponds to the extended phase and the eigenstate thermalization hypothesis is satisfied there. Concerning to the critical regime at the intermediate values of  $W$ , which is labeled by “critical” in Fig 2(a), the IPR has an intermediate value, which does not characterize the ETH ( $\text{IPR} \ll 1$ ) nor the strongly-localized state ( $\text{IPR} \sim 1$ ). Critical regime is larger for smaller  $\gamma$ , i.e., the long-range correlation of the disorder enhances the critical regime. For each phase, we shall see detailed scaling behaviors with the system size  $L$  in later discussions.

Here we should comment on the mobility edge. Actually for broad range of  $W$ , we have verified the existence of the mobility edge for both  $J_z = 0$  and  $J_z \neq 0$  cases. For all cases that we observed, the states in the vicinity of the band center are extended. This is in sharp contrast with the case of the short-range on-site disorder, in which all states are expected to be localized by Anderson localization. In fact, the previous works on some correlated disorders have gotten the same conclusions with ours [16], although the different parameter regime of  $\gamma$  was discussed.

We also calculated the entanglement-entropy (EE) for the half-filled groundstate by using Peschel’s method [22–25]. The numerical results are displayed in Fig. 2(b). The direct EE value is too subtle to quantify the three phases compared to the IPR result in Fig. 2(a). But, the

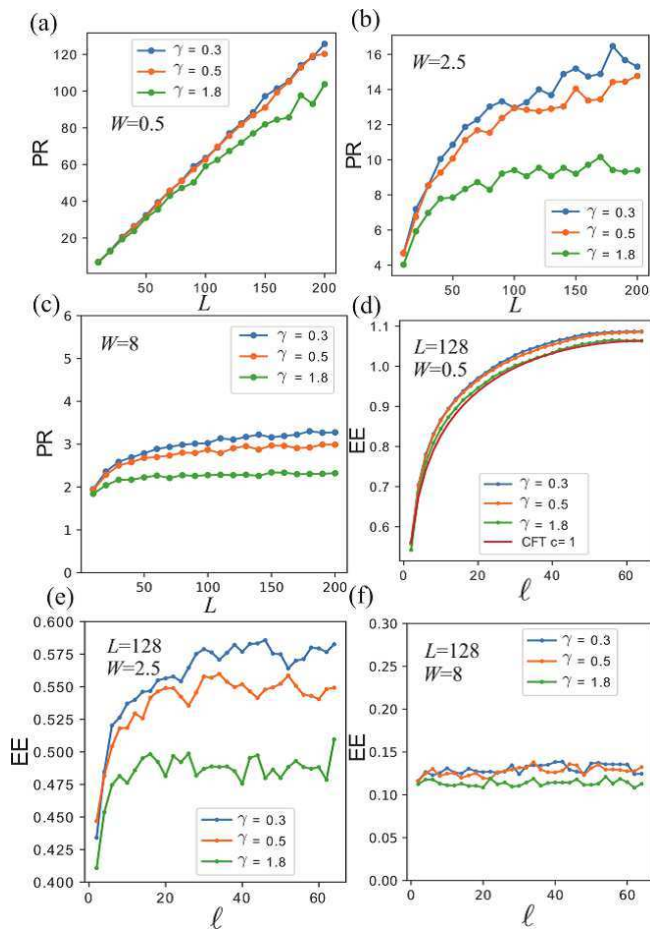


FIG. 3: System-size scaling of PR for  $W = 0.5$  (a),  $W = 2.5$  (b), and  $W = 8$  (c). Subsystem-size scaling of the half-filled groundstate EE for  $W = 0.5$  (d),  $W = 2.5$  (e), and  $W = 8$  (f). Both PR and EE exhibit characteristic behaviors in the ETH, critical and MBL states.

system-size scaling analysis gives useful insights on effects of disorder in the present model. See later discussion.

In order to observe the three phases, we qualitatively characterize each phase by investigating the system-size dependence of the participation ratio (PR),  $(PR) \equiv 1/(IPR)$ . In the recent study of an extended Aubry-Andre model [26], the scaling analysis of the PR was employed to distinguish three phases, which are similar to the present ones.

Our results of the system-size scaling of the PR are shown in Fig. 3 (a)-(c), in which three data correspond to the typical ETH, critical and localized states, respectively. For the ETH phase (Fig. 3 (a)), the PR apparently exhibits linear increase proportional to  $L$ , which is nothing but the behavior of the ETH phase. On the other hand for the critical phase (Fig. 3 (b)), the PR exhibits sharp increase for small  $L$ , but it tends to saturate as  $L$  is getting large. This is nothing but a character of the critical phase [26]. The degree of the increase depends on  $\gamma$ , i.e., for smaller  $\gamma$ , the increase is larger, i.e., delocalization

of the wavefunction is enhanced by the long-range correlation of the disorder. For the localized phase (Fig. 3 (c)), the PR does not increase as  $L$  is increased, which is the typical behavior of the localized state.

As the system-size dependence of the PR exhibits rather clear signals of localization and delocalization, it is interesting to investigate the subsystem-size scaling of the EE (SSEE) of the half-filled groundstate. The subsystem size is denoted by  $\ell (< L)$ . It is observed that the SSEE well captures the qualitative scaling behavior of the ETH and localization states [22], although sometimes strict scaling behavior is not obtained. In particular for ETH state, the numerical SSEE is expected to obey the following CFT scaling law [27],

$$S_{\text{CFT}}(\ell) = \frac{c}{6} \log[(L/\pi) \sin(\pi\ell/L)] + s_0, \quad (11)$$

where  $c = 1$ ,  $s_0 = S_{\text{data}}(\ell_0) - \frac{c}{6} \log[(L/\pi) \sin(\pi\ell_0/L)]$ , and  $\ell_0$  is the minimum size of the subsystem. Although  $S_{\text{CFT}}$  was originally proposed for the critical regime in the thermodynamic limit [27], we observe that it quantifies the ETH state by comparing it with the numerical SSEE for the finite size systems.

Figure 3 (d)-(f) are the results of the numerical SSEE for various  $(\gamma, W)$ , where we set  $L = 126$  and  $N_d = 2^3$ . In Fig. 3 (d), typical results for the ETH regime are obtained. The scaling results are very close to the CFT scaling function  $S_{\text{CFT}}$ . For the critical regime shown in Fig. 3(e), the SSEE slightly increases as  $\ell$  is increased [28], but the scaling of the SSEE does not satisfy the CFT scaling nor the area law (where  $S_{\text{SEE}} \sim \text{constant}$ ). For a fixed  $W$ , the smaller  $\gamma$  exhibits more increase of the SSEE as a function of  $\ell$ . This implies that the weak power-law decay of the disorder correlation (larger long-range correlation) enhances the increase of the SSEE. On the other hand, the localization regime as shown in Fig 3 (f) exhibits no area law scaling, i.e., the SSEE hardly increases as increasing  $\ell$ . This is nothing but the behavior of the localized state.

## V. XXZ MODEL: $J_z \neq 0$ CASE

Let us turn to the  $J_z \neq 0$  case, i.e., the interacting case. Here, we consider the case with  $J_z = 1$ , noticing that this case does not induce the anti-ferromagnetic order [density-wave phase in the fermionic picture]. As shown in the previous section, the ETH, critical and localized phases form in the non-interacting case due to the disorders with the long-range correlations. This is in sharp contrast to the standard model in which the random magnetic field is short-ranged. For a finite  $J_z$ , how the phase diagram changes is an interesting problem. In particular for small  $\gamma$  (long-range power-law decay) and moderate  $W$ , we investigate whether the observed critical phase is enhanced or not. To this end, we employ the exact diagonalization (ED) [29, 30]. To study localization of the system in detail, we use the multifractal analysis [17, 18] for various values of  $(\gamma, W)$ . This analysis is

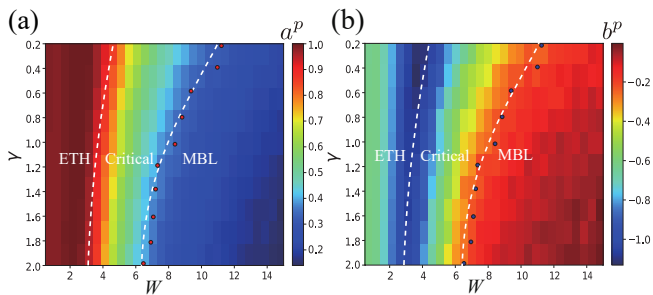


FIG. 4: (a)  $a^p$ -distribution in the multifractal analysis, and phase diagram in the  $(W, \gamma)$ -plain. The phase boundary between ETH and critical phase is determined by the minimum of  $b^p$ . The phase boundary between critical and MBL phases is determined by the finite-size scaling of the LSR and EE using data of various system sizes. The red dots are the transition points, which we numerically observed. (b) Detailed behavior of  $a^p$  and  $b^p$  for typical  $\gamma$ 's.

to find a Hilbert-space dimensional scaling for the participation entropies (PE) denoted by  $S_q$ . The quantity  $S_q$  is defined by  $q$ -th moment of wave-function coefficient of each eigenstate  $|\Psi^m\rangle = \sum_k \psi_k^m |k\rangle$ , where  $|k\rangle$  is computational basis, and  $|\Psi^m\rangle$  is the  $m$ -th many-body eigenstate. Then for  $|\Psi^m\rangle$ ,  $S_q$  is defined by

$$S_q^m = \frac{1}{1-q} \ln \left[ \sum_{k=1}^D |\psi_k^m|^{2q} \right], \quad (12)$$

where  $D$  is the dimension of the Hilbert space for the system size  $L$ . We focus on the case of  $q = 2$ , that is,  $S_2 = -\ln(\text{IPR})$ . The multi-fractal behavior is characterized by the fractional dimension  $a^p$  and logarithmic subleading correlation term  $b^p$ . These are obtained by a linear fitting such as  $\langle S_2 \rangle = a^p \ln D + b^p \ln(\ln D)$  [17], where the coefficients  $a^p$  and  $b^p$  are obtained by using the  $S_2$  data calculated for various system sizes. The values of  $a^p$  and  $b^p$  are known to characterize three phase: extended (ETH), critical and MBL [17, 18]. For  $a^p \approx 1$  and  $b^p < 0$ , the system is in the ETH phase, for  $0 < a^p < 1$  and  $b^p < 0$  the system is in the critical regime and for  $a^p \ll 1$  and  $b^p > 0$  the system is in the MBL state.

In the practical calculation, in order to perform the multi-fractal analysis, we first calculate the IPR defined by  $(\text{IPR})^m = \sum_k \langle k | \Psi^m \rangle$ , where  $|k\rangle$  is the many-body Fock state as reference bases. We calculate  $\langle \text{IPR} \rangle$  for the  $L = 8, 10, 12, 14$  and 16 systems. For the  $L < 16$  systems, data are obtained by averaging over 12.5% eigenstates of the Hilbert-space dimension in the vicinity of the band center and for  $10^2 - 10^4$  disorder realizations. For the  $L=16$  system, we use shift invert method and data are obtained by averaging over 250 eigenstates and for about 600 disorder realizations. By fitting the obtained IPR data in the linear form, we get the global phase diagram using obtained values of  $a^p$ . As shown in Fig. 4 (a) and (b), the values of  $a^p$  and  $b^p$  clearly capture the ETH-critical transition. Notably, we find that the transition

regime is located in the minimum of the  $b^p$  as shown in Fig. 4 (b), and also the transition line is almost independent of  $\gamma$ . On the other hand, it is not easy to determine the critical-MBL phase transition line only by the results of  $a^p$  and  $b^p$ . For large  $W$  regime, it is difficult to extract the genuine behavior of  $b^p$  in our system sizes. There, the value of  $b^p$  does not indicate clear positive value, although  $b^p$  almost approaches to zero. The zero-approaching behavior of  $b^p$ , however, gives a possible candidate of the phase transition line (or regime). Actually, as explained later, the phase boundary between the ETH and MBL phases can be extracted by the finite-size scaling analysis of the level-spacing analysis and entanglement entropy. By using these calculations, the phase boundary between ETH and MBL phases is determined in Fig. 4 (a). It should be emphasized that from our calculation, the multi-fractal analysis is efficient to characterize the phase boundary between ETH and critical phase. Since this calculation is obtained by various system size, the ETH and critical phase boundary is expected to be very close to that for the thermodynamic limit. It is useful to judge whether the critical phase survives in the thermodynamic limit or not. As shown in Fig. 4 (a), we found that the critical regime between the ETH and MBL phases is enlarged for small  $\gamma$ : the long-range power-law disorder. Here it should be remarked that the model with the white-noise disorder also exhibits the three phases. The observation of the behavior of  $b^p$  for different types of disorder are given in appendix A. The behavior of  $b^p$  for strong disorder depends on the type of disorder, therefore for strong disorder, estimation of  $b^p$  by itself is not sufficient to determine the transition to MBL phase in our numerics. The above findings are not observed in the case of the uniform disorder case [19], where in the thermodynamic limit, *the critical phase disappears and the direct phase transition of ETH-MBL is expected to occur*.

In addition, the global phase diagram of Fig. 4 (a) is fairly close to the non-interacting case ( $J_z = 0$ ) in Fig. 2 (a). Hence, we expect that even in the case of a finite  $J_z$ , the power-law disorder characterized by  $\gamma$  affects the interacting system similarly to the non-interacting system as long as the system does not have a quasi-long range order in the absence of disorders.

Here, we show how to extract the phase boundary between the critical and MBL phases. In order to corroborate the phase diagram in Fig. 4 (a), we calculate the average level-spacing ratio (LSR)  $\langle r \rangle$  [21, 32]. For calculating the LSR  $\langle r \rangle$ , we first obtain the spectrum  $\{E_i\}$  (in the ascending order). For each level spacing  $\{E_i\}$ , we define  $r^k = [\min(\delta^{(k)}, \delta^{(k+1)})] / [\max(\delta^{(k)}, \delta^{(k+1)})]$ , where  $\delta^{(k)} = E_{k+1} - E_k$ . Value of  $\langle r \rangle$  is obtained by averaging over hybrid samples obtained by disorder realizations and 12.5% eigenstates of the Hilbert space dimension in the vicinity of the band center. For the  $L=16$  system, we use shift invert method. This calculation gives the clear result of  $\langle r \rangle$  [32]. The value of  $\langle r \rangle$  characterizes the ETH and MBL phases; for the ETH phase,  $\langle r \rangle \sim 0.53$  (Gaus-

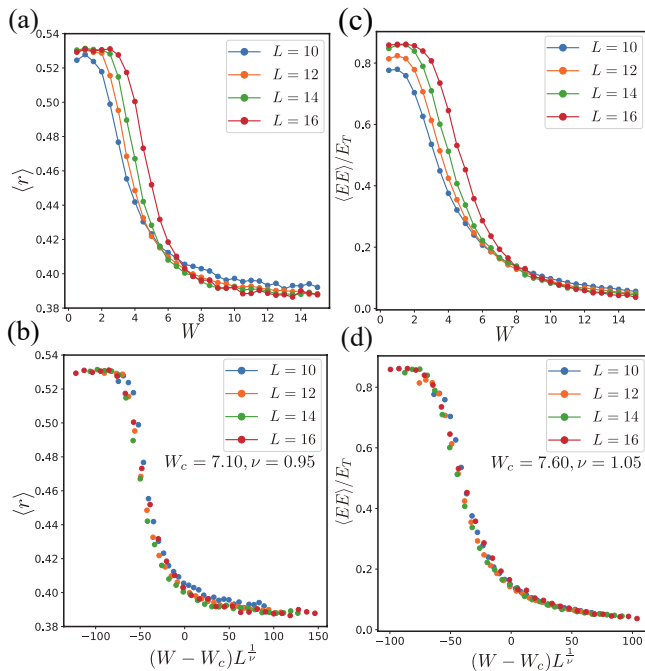


FIG. 5: (a) Average LSR  $\langle r \rangle$  for  $\gamma = 1.6$ . (b) Finite-size scaling of  $\langle r \rangle$  for  $\gamma = 1.6$ . Critical value of  $W$  [ $W_c$ ] is estimated as  $W_c = 7.10$ . (c) Average entanglement entropy  $\langle EE \rangle$  for  $\gamma = 1.6$ , scaled by the Page value  $E_T = 0.5(L \ln 2 - 1)$  [31]. (d) Finite-size scaling of  $\langle EE \rangle$  for  $\gamma = 1.6$ .

sian orthogonal ensemble), for the MBL,  $\langle r \rangle \sim 0.386$  (Poisson random matrix ensemble), and the intermediate values of  $\langle r \rangle$  indicates the critical phase. Figures 5 (a) show the  $W$ -dependence of  $\langle r \rangle$  for a typical  $\gamma$  and various system sizes. All data move from  $\langle r \rangle \sim 0.53$  to  $\langle r \rangle \sim 0.386$  as  $W$  increases. Globally, the all data exhibit behavior of the ETH-MBL transition. Notably, the results obtained for various system sizes shown in Figs. 5 (a) tend to intersect with each other at a single point,  $W \sim 7.10 \equiv W^c$ . Hence, we conclude that the estimated  $W^c$  is the phase transition point separating the ETH-critical phases. Furthermore, we extracted the critical exponent  $\nu$  by using  $W_c$  in Fig. 5(b). We obtained  $\nu = 0.95$ - $1.05$ , which clearly breaks the Harris criterion,  $\nu = 2$  [33]. Our value  $\nu = 0.91$  is almost the same with the value obtained in the conventional MBL phase transition [32]. We conclude that the LSR can capture the ETH-critical phase transition by using the finite-size scaling of the LSR.

In addition, the EE is calculated to complement the level-spacing analysis. By using the subsystem with  $L/2$  system size, the EE,  $S_A$ , is calculated as  $S_A = -\text{Tr}[\rho_A \log \rho_A]$ , where  $\rho_A$  is the partial density matrix of the subsystem that is obtained from a many-body eigenstate of the full system. The system size dependence for typical  $\gamma = 1.6$  is displayed in Fig. 5 (c). Here, similarly to the LSR, the calculations of the EE intersect with each other at a single point,  $W \sim 7.60 \equiv W^c$ , which is very

close to the value of the LSR. The scaling behavior of the EE is plotted in Fig. 5 (d). Here, the critical exponent  $\nu$  is very close to the value of  $\nu$  in the LSR. From above observation, we found that the critical-MBL phase transition can be clearly observed by both the LSR and EE finite-size scaling analysis.

From the results of the multi-fractal analysis, LSR and EE, we conclude that in the present power-law disorder model, the transition points of the ETH-critical and critical-MBL are clearly different, and the critical region survives even in the thermodynamic limit.

## VI. DYNAMICS OF ENTANGLEMENT ENTROPY AND IMBALANCE: $J_z \neq 0$ CASE

In this section, we investigate the dynamics of the EE and imbalance to see characteristics of the three phases observed in Sec. V. For the finite- $J_z$  system, the EE is obtained from a time-dependent many-body state of the full system. In general, the dynamics of the EE is used to distinguish the MBL state from other states such as Anderson localized, ETH, and critical phases, as the EE exhibits a very slow evolution in the MBL state. In particular, if an initial state is a local product state such as the Néel state, the time evolution of the state accompanies a change of the EE caused by its dephasing [34–36]. It is known that such dephasing is strong in the MBL states, and as a result, increase of EE is very slow. Figure 6 (a) is the numerical results of the dynamics of the EE for various  $\gamma$  and  $W$ . Here, we employed the Néel state as an initial state. For small  $W = 0.5$ , which corresponds to the ETH state,  $EE \propto t$  and it saturates to a finite value close to unity. This is nothing but a ballistic evolution of the EE. On the other hand for the MBL regime ( $W = 15$ ), the increase of the EE is very slow, i.e.,  $EE \propto t^{1/6}$ . We also observe a characteristic  $\gamma$ -dependence of the time evolution of the EE, that is, for smaller- $\gamma$  (long-range correlation of disorder), system exhibits weaker dephasing in the MBL phase. This tendency is clearly observed from the data of the EE for the  $J_z = 0$  and  $J_z = 1$  cases, as we show  $\delta S_A \equiv S_A(J_z = 1) - S_A(J_z = 0)$  in Fig. 6 (b). Therefore, the power-law disorder can control the rate of increase of the EE. Such control may be possible in recent cold-atom experimental systems [4–7]. Finally for the critical regime with  $W = 5.0$ , the EE displays time evolution that is in-between of the ETH and MBL states. In the intermediate temporal region,  $EE \propto t^{1/2}$ , and its increase tends to slow for  $t > e^3$ . Anyway, the three regimes exhibit three different behaviors of the EE, which supports the results obtained from the IPR and level-spacing analysis in Sec. V. In addition, for different initial states, the EE dynamics again exhibits different behavior for each of the three phases. The results are shown in Appendix B.

Finally, we study the time evolution of the imbalance of the  $z$ -component of the system spin, which is defined

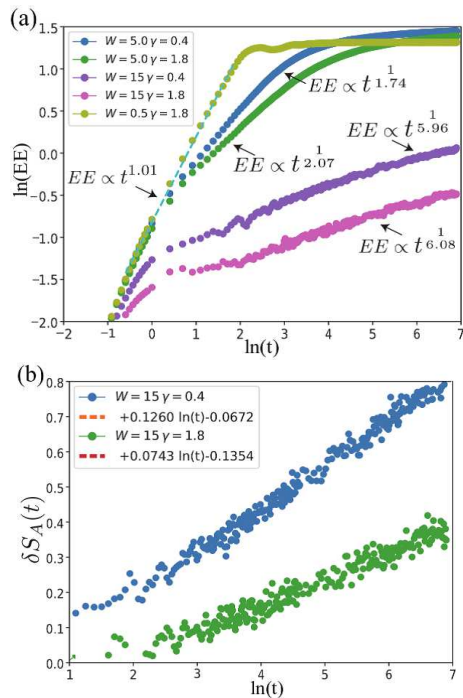


FIG. 6: (a) Time evolution of entanglement entropy for various points in  $(\gamma, W)$ . System size is  $L = 18$ , and the open boundary condition is employed. Data of 50 disorder realizations are averaged for each point in  $(\gamma, W)$ . (b) The difference of the EE between the  $J_z = 0$  and  $J_z = 1$  cases. Shown results are for MBL regime ( $W = 15$ ).

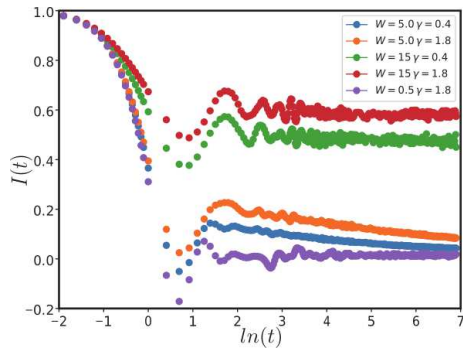


FIG. 7: Time evolution of the spin z-component imbalance for ETH, critical and MBL phases. Each phase exhibits its typical behavior.

as

$$I(t) = (S_o^z - S_e^z)/(S_o^z + S_e^z),$$

where  $S_o^z = \sum_{j \in \text{odd}} S_j^z$  and  $S_e^z = \sum_{j \in \text{even}} S_j^z$ . For the numerical study, we employ the Néel state as the initial state, and we average the calculations over 50 disorder realizations. Figure. 7 displays results of the averaged  $I$  for typical values  $(\gamma, W)$  corresponding to the ETH, critical and MBL phases. For  $W = 0.5$ ,  $I(t)$  approaches

to the vanishing value after oscillation. This behavior is expected as the system is in the ETH state. On the other hand for  $W = 15.0$ ,  $I(t)$  keeps a finite value as  $t \rightarrow \infty$  for both  $\gamma = 0.4$  and  $1.8$  cases. This result obviously indicates that the system is in the MBL state. The case  $W = 5.0$  exhibits the behavior of  $I(t)$  that is in-between of the ETH and MBL states. All the above calculations of  $I(t)$  support the conclusion obtained so far.

## VII. CONCLUSION

In this work, we have systematically investigated effects of power-law correlated disorder not only for the non-interacting case but also for the system with the many-body interactions. We clarified that for both the non-interacting and interacting systems, the critical phase exists between the ETH and MBL phases and it is enhanced by the long-range correlations of the disorder. In particular for the MBL system, we obtained the detailed phase diagram by making use of the multifractal analysis, LSR and EE calculations. The multifractal analysis is efficient to determine the ETH-critical phase boundary while the LSR and EE are useful for determining the critical-ETH phase boundary. Under the power-law disorder, the critical phase seems to survive even in the thermodynamic limit. This is in sharp contrast to the well-studied MBL systems with short-range disorders [19]. Also, the regime of the critical phase is strongly affected by the properties of the long-range correlations.

Finally, we investigated the dynamics of the EE under the power-law disorder. For the critical and MBL parameter regimes, the EE dynamics exhibits different behavior in the time evolution. The time evolution of the EE depends on the properties of the long-range correlations of the disorder as the other observed physical quantities do. This result indicates that the power-law disorder has potential ability to control the evolution of the EE. Such a control of the correlations in the disorders is feasible in recent real experiments on cold atoms. Therefore, we expect that physical phenomena originating from the long-range disorders will be observed by experiments on ultra-cold atoms, trapped ions, etc.

### Appendix A: Calculations of $b^p$ in $\langle S_2 \rangle$ for various types of disorder

Here, we show the detail calculations of  $b^p$  in the multifractal analysis. We would like to verify the utility of  $b^p$ 's multi-fractal analysis to determine the phase diagram in finite systems. In fact, we found that the utility depends on the types of disorder.

We calculated for  $W$ -dependence of  $b^p$  for the following three cases; (i) uniform random disorder,  $\in [-W, W]$ , (ii) white noise,  $\sum W_i = 0$ ,  $\sum \frac{1}{L}(W_i - \langle W \rangle)^2 = \frac{W^2}{12}$ , and (iii) Power law disorder with  $\gamma = 0.8$ . The results are shown

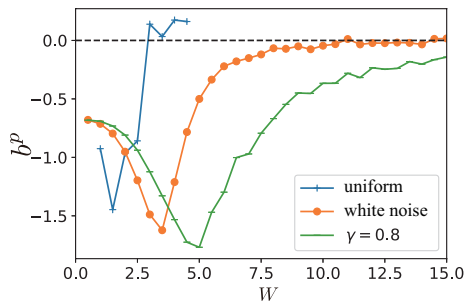


FIG. A.1:  $W$ -dependence of  $b^p$  for various types of disorder. Values of  $b^p$  are estimated by using the data up to  $L = 16$  system size.

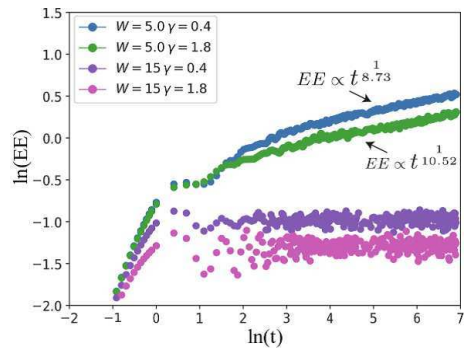


FIG. B.1: Time evolution of the entanglement entropy for various  $(\gamma, W)$ . System size  $L = 18$ , and open boundary condition is used. Data are obtained by averaging over 50 disorder realizations.

in Fig. A.1. In the case of the uniform disorder, the value of  $b^p$  becomes sufficiently positive for large  $W$ . This indicates that  $b^p$  correctly characterizes the MBL phase transition even in the system of  $L = 16$ . On the other hand for the cases of both the white noise and power-law disorder,  $b^p$  does not have a positive value in the  $L = 16$  system size even for large  $W$ , although the value of  $b^p$  is fairly close to zero for the white noise, and takes positive value sometimes. These results indicate that calculation of the parameter  $b^p$  by itself is not sufficient for characterizing MBL phase transition at least for the system size  $L = 16$ .

## Appendix B: Time evolution of entanglement entropy for a domain wall initial state

We study time evolution of the EE and related physical quantities for a different initial state. We set a domain wall configuration: up spin are set from  $j = 1$  to  $j = L/2$  and down spin are set from  $j = L/2 + 1$  to  $j = L$ , therefore the kink is located between  $L/2$  and  $L/2 + 1$ -th sites. For the critical and MBL phase regimes, the numerical results are shown in Fig. B.1. Here we found that in the critical phase, the EE exhibits logarithmic growth in the time evolution and the evolution rate is larger for smaller  $\gamma$ . On the other hand in the MBL phase, the EE saturates to a finite values after a finite period, and the saturating value is larger for smaller  $\gamma$ .

- 
- [1] R. Nandkishore and D. A. Huse, *Annu. Rev. Condens. Matter Phys.* **6**, 15 (2015).
- [2] D. A. Abanin and Z. Papić, *Annalen der Physik* **529**, 1700169 (2017).
- [3] F. Alet and N. Laflorencie, *Comptes Rendus Physique* **19**, 498 (2018)
- [4] M. Schreiber, S. S. Hodgman, P. Bordia, H. P. Lüschen, M. H. Fischer, R. Vosk, E. Altman, U. Schneider and I. Bloch, *Science* **349**, 842 (2015).
- [5] J. -Y. Choi, S. Hild, J. Zeiher, P. Schaus, A. Rubio-Abadal, T. Yefsah, V. Khemani, D. A. Huse, I. Bloch and C. Gross, *Science* **352**, 1547 (2016).
- [6] A. Lukin, M. Rispoli, R. Schittko, M. E. Tai, A. M. Kaufman, S. Choi, V. Khemani, J. Léonard and M. Greiner, *Science* **364**, 256 (2019).
- [7] M. Rispoli, A. Lukin, R. Schittko, S. Kim, M. E. Tai, J. Léonard and M. Greiner, *Nature* **573** 385 (2019).
- [8] X. Deng, G. Masella, G. Pupillo, and L. Santos, arXiv:1912.08131 (2019).
- [9] S. Schiffer, J. Wang, X. Liu, and H. Hu, arXiv:1908.04031 (2019).
- [10] P. Sierant, K. Biedro, G. Morigi, and J. Zakrzewski, *SciPost Phys.* **7**, 008 (2019).
- [11] F. Evers and A. D. Mirlin, *Rev. Mod. Phys.* **80**, 1355 (2008).
- [12] K. Takeda and I. Ichinose, *Nucl. Phys. B* **663**, 520 (2003).
- [13] T. Kaya, *Eur. Phys. J. B* **55**, 49 (2007).
- [14] H. Shima, T. Nomura, and T. Nakayama, *Phys. Rev. B* **70**, 075116 (2004).
- [15] I. F. Dos Santos, F. A. B. F. De Moura, M. L. Lyra, and M. D. Coutinho-Filho, *J. Phys. Condens. Matter* **19**, 476213 (2007).
- [16] A. Croy, P. Cain, and M. Schreiber, *Eur. Phys. J. B* **82**, 107 (2011).
- [17] N. Mace, F. Alet, and N. Laflorencie, *Phys. Rev. Lett.* **123**, 180601 (2019).
- [18] W. Yucheng, L. Xiong-jun, and Y. Dapeng, arXiv:1910.12080 (2019).
- [19] V. Khemani, S. P. Lim, D. N. Sheng, and D. A. Huse, *Phys. Rev. X* **7**, 021013 (2017).
- [20] H. A. Makse, S. Havlin, M. Schwartz, and H. E. Stanley, *Phys. Rev. E* **53**, 5445 (1996).
- [21] J. Janarek, D. Delande, J. Zakrzewski, *Phys. Rev. B* **97**, 155133 (2018).
- [22] I. Mondragon-Shem and T. L. Hughes, *Phys. Rev. B* **90**, 104204 (2014).
- [23] I. Mondragon-Shem, M. Khan, and T. L. Hughes, *Phys. Rev. Lett.* **110**, 046806 (2013).

- [24] I. Peschel, *J. Phys. A: Math. Gen.* **36**, 12 (2003).
- [25] I. Peschel and V. Eisler, *J. Phys. A: Math. Theor.* **42**, 504003 (2009).
- [26] F. Liu, S. Ghosh, and Y. D. Chong, *Phys. Rev. B* **91**, 014108 (2015).
- [27] Calabrese and Cardy *J. Stat. Mech.* **P06002** (2004).
- [28] This behavior is reminiscent to the previous study [26].
- [29] P. Weinberg and M. Bukov, *SciPost Phys.* **2**, 003 (2017).
- [30] P. Weinberg and M. Bukov, *SciPost Phys.* **7**, 020 (2019).
- [31] D. N. Page, *Phys. Rev. Lett.* **71**, 1291 (1993).
- [32] D. J. Luitz, N. Laorencie, and F. Alet, *Phys. Rev. B* **91**, 081103 (2015).
- [33] A. B. Harris, *J. Phys. C: Solid State Phys.* **7**, 1671 (1974).
- [34] M. Serbyn, Z. Papić, and D. A. Abanin, *Phys. Rev. Lett.* **110**, 127201 (2013).
- [35] A. Chandran, I. H. Kim, G. Vidal, and D. A. Abanin, *Phys. Rev. B* **91**, 085425 (2015).
- [36] D. A. Huse and V. Oganesyan, *Phys. Rev. B* **90**, 174202 (2014).